

THE PHYSICS OF TYPE Ia SUPERNOVA LIGHT CURVES. I. ANALYTIC RESULTS AND TIME DEPENDENCE

PHILIP A. PINTO¹

Steward Observatory, University of Arizona, Tucson, AZ 85721; ppinto@as.arizona.edu

AND

RONALD G. EASTMAN²

Lawrence Livermore National Laboratory, Livermore, CA 94550; reastman@llnl.gov

Received 1999 October 4; accepted 1999 October 5

ABSTRACT

We develop an analytic solution of the radiation transport problem for Type Ia supernovae (SNe Ia) and show that it reproduces bolometric light curves produced by more detailed calculations under the assumption of a constant-extinction coefficient. This model is used to derive the thermal conditions in the interior of SNe Ia and to study the sensitivity of light curves to various properties of the underlying supernova explosions. Although the model is limited by simplifying assumptions, it is adequate for demonstrating that the relationship between SNe Ia maximum-light luminosity and rate of decline is most easily explained if SNe Ia span a range in mass. The analytic model is also used to examine the size of various terms in the transport equation under conditions appropriate to maximum light. For instance, the Eulerian and advective time derivatives are each shown to be of the same order of magnitude as other order v/c terms in the transport equation. We conclude that a fully time-dependent solution to the transport problem is needed in order to compute SNe Ia light curves and spectra accurate enough to distinguish subtle differences of various explosion models.

Subject headings: diffusion — radiative transfer — stars: interiors — supernovae: general

1. INTRODUCTION

The bolometric light curve is the simplest and most direct manifestation of Type Ia supernovae (SNe Ia). For many years it had been assumed that all Type Ia supernovae were identical explosions, with identical light-curve shapes and peak luminosities (cf. Woosley & Weaver 1986). While evidence for this uniformity in the data was never terribly convincing, the use of SNe Ia as the primary “standard candles” for cosmological distance measurement provided a powerful incentive for assuming this homogeneity. This in turn lead naturally to a search for an explosion model that might produce identical displays from the diversity of progenitors supplied by stellar evolution.

It became clear from the light curve’s rapid evolution that a relatively low-mass object was involved—one with a short radiative diffusion time (Arnett 1982). The result of this search is what one might call the present “standard model”: the thermonuclear incineration of a carbon-oxygen white dwarf at the Chandrasekhar mass (see Woosley & Weaver 1986, Arnett 1996 for details of this search and a review of various models). The Chandrasekhar mass provides a point of convergent evolution for various progenitor systems, offering a natural explanation of the assumed uniformity of display. The high densities attained at the centers of these objects provide a mechanism (as ill-defined as it may be at present) for their ignition, as well.

With the coming of age of various supernova searches (Evans, van den Bergh, & McClure 1989; Hamuy et al. 1993; Barbon et al. 1993; Pollas 1994), there has recently been an explosion in the availability of high-quality data. It is now generally recognized that SNe Ia exhibit a variety of

light-curve shapes, peak luminosities, and maximum-light spectra. Perhaps most significant has been the discovery of various regularities in the light-curve data, the most famous of which we will call the “luminosity-width relation” (hereafter LWR): the brightest supernovae have the broadest light-curve peaks (Phillips 1993). There is also significant evidence (Vacca & Leibundgut 1996) that the decline at late times is more gradual in the brighter supernovae.

This additional information provides new clues to the nature of these explosions. We develop here, from first principles, a theoretical framework for examining the formation of SNe Ia light curves and extracting underlying properties of the explosions. There have been a number of studies of the light-curve problem in SNe Ia. In analytic work, Arnett (1982, 1996) made various assumptions (discussed below) that misrepresented the nature of energy deposition by radioactive decay. The analytic results in this paper are a generalization of his work.

Various numerical studies of the light-curve problem (Harkness 1991; Höflich, Khokhlov, & Wheeler 1995 and references therein; Weaver, Axelrod, & Woosley 1980) have appeared in the literature. All of these have taken specific instances of explosion models and computed, to various degrees of approximation, the resulting light curves. None, however, have explored the effects of varying individual properties of the underlying explosions while keeping all others fixed. In this work, we will employ a rather less sophisticated treatment of the transfer physics than previous authors have used and instead make a more systematic investigation of the effects of different explosions. The simplified explosions we employ will thus not reflect any self-consistent model of the supernova phenomenon but will make the effects of changing various parameters more explicit.

¹ Lawrence Livermore National Laboratory, Livermore, CA 94550.

² Department of Astronomy and Astrophysics, University of California, Santa Cruz, Santa Cruz, CA 95064.

In the first section of this work, we derive an analytic solution for the comoving frame transfer equation in homologous expansion, which relaxes the assumptions made by Arnett (1982). In the next section, we examine the effects on the bolometric light curve of varying the properties of the underlying explosions. We use the solution from § 1 in the third section to examine the relative importance of various terms in the equations and the suitability of various approximations that have appeared in the literature. The analytic solution also provides an important check on the accuracy of subsequent numerical solutions (Pinto & Eastman 2000a).

The postexplosion dynamics of SNe Ia, which determine the density and velocity structure, are quite simple. As in all strong point explosions, the expansion becomes homologous. After a time that is short compared with the bolometric rise time, the velocity gradient becomes equal everywhere to the reciprocal of the elapsed time. The density structure is quite smooth, with a density profile not very different from $\rho \propto \exp(-4v/v_0)$ [with v_0 some typical velocity $\propto (E/M)^{1/2}$]. There is usually a small amount of high-velocity material at the surface, in which the density drops more rapidly; as this material is largely transparent long before the supernova is observed, we may ignore this detail. To a surprising degree, all explosion models to date have this relatively simple structure. Thus, the dynamics can be specified by the explosion energy and the mass of the ejecta (in most models, the progenitor is completely disrupted).

The other defining attributes of the explosion are in the composition of the ejecta. Since it is radioactive nickel that leads to any significant optical display, the amount of ^{56}Ni and the depth to which it is buried in the ejecta will obviously affect the light curve. The composition also affects the opacity, obviously a determining parameter in a problem concerned with the escape of radiation. In the next paper of this series, we will examine the frequency distribution of the opacity in a Type Ia supernova explosion and details of the way in which energy diffuses from the center to the surface (Pinto & Eastman 2000a).

We will thus define a supernova by its total mass, explosion energy, ^{56}Ni mass, and opacity, allowing for variations in the spatial distribution of the last two. With a simple means of producing a light curve from these parameters, one may eventually be able to turn the problem around and use the light-curve model to extract values for these parameters from observations of SNe Ia.

We find that, with the exception of the total mass, variations in any of these basic parameters lead to a behavior of the light curve that is in the *opposite sense* of the LWR. Varying the total mass can lead to a sequence of light curves in which the LWR behavior is reproduced, but to date, a viable model for supernovae with varying masses has not been found. The full richness of SN Ia light-curve behavior might be obtained from Chandrasekhar-mass explosions. These analytical models assume a constant opacity. Höflich et al. (1995 and references therein) have suggested that it is the temperature dependence of the opacity that is the primary factor in determining the light-curve shape. While we show in a subsequent paper that these models significantly overestimate this temperature dependence (Pinto & Eastman 2000a), the idea is still probably correct, and we provide a simple demonstration of this effect. The fact that a constant-opacity solution can reproduce the observed

behavior does, however, suggest that the total mass of the explosion could be a natural and simple explanation.

This is the first paper of a series. The next paper (Pinto & Eastman 2000a, hereafter Paper II) explores the physics of radiation transport in SNe Ia and the nature of the opacity. The third (P. Pinto & R. Eastman 2000b, in preparation) examines the nature of the secondary maximum in infrared colors. Subsequent papers will systematically explore the light-curve and spectrum properties of specific models for Type Ia supernovae.

2. A SCHEMATIC TYPE Ia SUPERNOVA

In this section we develop a simple analytic model for the thermal evolution and light curve of a SN Ia. This will prove useful for estimating physical conditions in the ejecta at various times after explosion and for illustrating the effect that changes in opacity, mass, energy deposition, and explosion energy have on the bolometric light curve.

The ejecta of SNe Ia form an opaque, expanding sphere into which energy is deposited by radioactive decay at an exponentially declining rate. Because the sphere is initially so opaque, this energy is converted into kinetic energy of expansion on a hydrodynamic timescale.³ At the earliest stages, the ejecta is so optically thick that the time it takes radiation to diffuse out is much longer than the elapsed time. The luminosity is therefore initially quite small. As time passes, the ejecta become more dilute and the diffusion time drops below the (ever-increasing) elapsed time. Since the rate of energy input declines exponentially with time, there is a peak in the light curve as soon as the injected energy has an appreciable chance to escape conversion to kinetic energy—when the diffusion time becomes comparable to the elapsed time. While the fraction of deposited energy that escapes conversion will continue to increase, this is more than offset by the decreasing energy deposition rate.

Shortly after this peak, there will be a considerable amount of radiation still trapped and diffusing outward. Since the energy deposition rate is so rapidly declining, the luminosity will, for a time, exceed the rate of deposition, until the supernova empties itself of this excess stored energy. Finally, as the rate of energy deposition, now from cobalt decay, declines more slowly and the diffusion time becomes small, the luminosity becomes equal to the instantaneous deposition rate. There are thus two milestones in the light curve. The first occurs near peak when the luminosity first rises above the rate of energy deposition. The second occurs when the excess, stored energy is exhausted and the luminosity falls to equal the instantaneous deposition. The elapsed time and the rate of deposition are easily determined. The first is obvious and the second comes from the decay of ^{56}Ni to ^{56}Fe and the transport of γ -rays—fairly simple physics. Determining the diffusion time is a far more complex matter, and most of the difficulty in producing synthetic light curves and spectra arises from correctly characterizing the transport and escape of thermalized radiation.

Arnett showed in two elegant papers (Arnett 1980, 1982) that the ideas expressed above could be demonstrated by a simple analytic model that accounts for the deposition and

³ For a point explosion like a SN Ia, the hydrodynamic timescale is comparable to the elapsed time.

escape of radiation from the expanding ejecta. This model predicted a bolometric light curve that was generally in good agreement with observed SN Ia behavior. Starting from the thermodynamics of the trapped radiation, he showed that the luminosity at peak was equal to the instantaneous energy deposition rate under the assumption of constant opacity, and thus, the first milestone occurs near peak bolometric luminosity. A number of assumptions were made that for a first attempt were quite reasonable, but that rendered suspect the precise predictions for any particular model explosion. These included a constant-density structure, a constant opacity in both space and time, and the requirement that the radial distribution of the energy deposition was identical to that of the thermal energy. Thus, while he could vary the expansion velocity and the total mass, the effects of varying the structure of the ejecta and of a realistic energy-deposition profile were beyond examination. In mathematical terms, Arnett's solution was an eigenfunction expansion from which only the fundamental mode is retained. We shall have more to say on this later.

We take a no-frills approach similar to Arnett's (1982), while relaxing some of his more limiting assumptions so as to be able to address additional questions, such as how the density structure and distribution of radioactive isotopes are manifested in the bolometric light curve.

We start by writing down the first two frequency-integrated moments of the time-dependent, comoving frame radiative transport equation in spherical geometry. The first moment equation, for the radiation energy density, can be written correct to all terms $O(v/c)$ as (e.g., Mihalas & Mihalas 1984)

$$\frac{DE}{Dt} + \frac{1}{r^2} \frac{\partial}{\partial r} (r^2 F) + \frac{v}{r} (3E - P) + \frac{\partial v}{\partial r} (E + P) = \int_0^\infty (4\pi\eta_\nu - c\chi_\nu E_\nu) dv. \quad (1)$$

The second frequency-integrated moment, for the radiation momentum, is

$$\frac{1}{c^2} \frac{DF}{Dt} + \frac{\partial P}{\partial r} + \frac{3P - E}{r} + \frac{2}{c^2} \left(\frac{\partial v}{\partial r} + \frac{v}{r} \right) F = -\frac{1}{c} \int_0^\infty \chi_\nu F_\nu dv. \quad (2)$$

Here, E , F , and P are the zeroth, first, and second frequency-integrated moments of the radiation field: the energy density, the flux, and the (isotropic) radiation pressure. The quantity χ_ν is the extinction coefficient, and η_ν is the volume emissivity. These are formidable equations to solve directly (cf. Eastman & Pinto 1993, among others); our goal here is to obtain a simple, approximate solution.

The first and most important assumption we will employ is that the expansion is homologous. As already described, SNe Ia are strong point explosions; homologous expansion will be an excellent approximation if the energy released by ^{56}Ni decay does not strongly affect the dynamics of the expansion. The energy available from ^{56}Ni decay is 3×10^{16} ergs g^{-1} . This corresponds to the kinetic energy of a gram of material traveling at nearly 2500 km s^{-1} , or, equivalently, a velocity increment of the same magnitude over the velocity initially imparted by the explosion. The significantly greater decay energy available from decay all

the way to ^{56}Fe is less relevant, as most of the ^{56}Co decay energy is emitted at times when the supernova is becoming optically thin. Since the observed expansion velocity of SNe Ia is in excess of 10^4 km s^{-1} , we expect that this additional source of energy will have a modest, but perhaps not completely negligible, effect upon the velocity structure. Furthermore, as the time to maximum light, t_{max} , is observed to be at least twice as large the ^{56}Ni decay time, most of the hydrodynamic effect of ^{56}Ni decay will have occurred prior to a supernova's discovery. If we take the ejecta's density structure from an explosion calculation that has allowed this additional energy to accelerate the ejecta for the first few days, we will have taken this effect sufficiently into account. We will therefore take the outer edge of the supernova, or at least of a fiducial mass shell that contains virtually all of the mass, to be at a velocity v_{max} and a radius

$$R(t) = R_0 + v_{\text{max}} t, \quad (3)$$

where R_0 is the initial radius of the progenitor. For this type of expansion law, there is an associated timescale

$$t_{\text{sc}} = R_0/v_{\text{max}}, \quad (4)$$

which will be one of the parameters of the solution.

A major simplification is the so-called *Eddington approximation*, wherein the radiation field is isotropic everywhere: $E = 3P$. This is certainly valid during the early, optically thick stages of evolution, but breaks down when the ejecta become transparent. The error that this assumption introduces at late times affects principally the energy distribution (the radiation energy density) and has much less effect on the bolometric luminosity, which is the only link this simple analytic model has to SN Ia observations. We note in passing that this assumption has dire consequences for the calculation of the energy deposition, where the deposition rate is proportional to the γ -ray energy density and not the flux.

It is important in this context to distinguish the Eddington approximation from the diffusion approximation. The diffusion approximation results from expanding the optical depth variation of the source function (usually assumed to be the Planck function in the diffusion regime) in a power series in τ and retaining only the first term. This implies that the radiation field is isotropic *and* that the flux is proportional to $dB/d\tau$. The Eddington approximation amounts to performing a one-point Gaussian quadrature of the specific intensity in forming angular moments of the radiation field. While the radiation field is thus assumed to be isotropic, the flux can depart greatly from $dB/d\tau$ in regions of low optical depth and far more closely approximates a complete solution. Most importantly, the Eddington approximation retains the wavelike character of equations (1) and (2) with wave speed c while the diffusion approximation propagates radiation in optically thin regions with infinite speed. See, for example, Mihalas (1978) for further discussion of this point.

At the temperatures and densities of maximum-light SNe Ia, the gas energy density is less than the radiation-field energy density by a large factor. The radiation-field energy density is

$$\rho_{\text{rad}} \equiv aT^4 \sim 1210 \left(\frac{T}{2 \times 10^4 \text{ K}} \right)^4, \quad (5)$$

which greatly exceeds both the thermal kinetic energy density

$$\rho e_{\text{kin}} \equiv \frac{3\rho N_A}{2A} (i+1)kT \sim 0.4 \left(\frac{\rho}{10^{-12} \text{ g cm}^{-3}} \right) \times \left(\frac{T}{2 \times 10^4 \text{ K}} \right) \left(\frac{A}{56} \right) \quad (6)$$

and the ionization energy density

$$\rho e_{\text{ion}} \equiv \frac{\rho N_A}{A} \langle E \rangle \sim 0.5 \left(\frac{\rho}{10^{-12} \text{ g cm}^{-3}} \right) \left(\frac{\langle E \rangle}{30 \text{ eV}} \right) \left(\frac{A}{56} \right), \quad (7)$$

where N_A is Avogadro's number, A is the mean mass per nucleon, i is the average ionization, and $\langle E \rangle$ is the mean ionization energy.

The dominance of radiation over internal energy permits us to ignore the gas internal energy and set

$$\int_0^\infty (4\pi\eta_\nu - c\chi_\nu E_\nu) d\nu = \epsilon, \quad (8)$$

where ϵ is the volume rate of γ -ray deposition. Equation (8) is equivalent to saying that as soon as high-energy radiation from decay is absorbed, it is immediately reradiated as thermal emission. The mechanism by which this happens is collisional: γ -rays Compton scatter, producing high-energy electrons, which then rapidly transfer their energy to the plasma. This occurs on a timescale that is short compared with any other timescale important to the problem of energy transport.

While the escape of radiation from the supernova during the peak of the light curve occurs on timescales much longer than the light-crossing time, the radiation field changes considerably on a hydrodynamic timescale. Following the discussion in Mihalas & Mihalas (1984), in order to ensure the correct radiation energy balance, all terms to $O(v/c)$ must be retained in the radiation energy equation (eq. [1]). However, in the frequency-integrated radiation momentum equation, (eq. [2]), it is appropriate on a fluid-flow timescale to discard all time- and velocity-dependent terms. This difference in treatment is intuitively evident when one realizes that we are vitally interested in determining the energy density and its flow within the supernova, yet the radiation momentum has little effect upon the supernova's dynamics after the first few days. The radiation momentum equation is thus reduced to the familiar diffusion form

$$F = -\frac{c}{3\chi} \frac{\partial E}{\partial r}, \quad (9)$$

where χ is an appropriately defined frequency-averaged mean opacity. We note once again that this result is valid beyond the diffusion regime. Even when the mean free path of photons becomes large, it is justifiable to ignore the time- and velocity-dependent terms in the momentum equation (see Mihalas & Mihalas 1984 for further discussion of this point).

Using this and the previous approximations in the radiation energy equation, the transport equation becomes

$$\frac{DE}{Dt} - \frac{c}{3r^2} \frac{\partial}{\partial r} \left(r^2 \frac{\partial E}{\partial r} \right) + \frac{4\dot{R}}{R} E = \epsilon. \quad (10)$$

In general, equation (10) is too complicated to solve analytically. However, for certain conditions specified below, the spatial and temporal parts of the solution may be separated, and equation (10) reduced to two ordinary differential equations.

It is convenient to homologously scale all of the remaining quantities in terms of the time t and $x = r/R$, the (dimensionless) fractional radius. Since the gas is radiation dominated, $E \propto R^{-4} \propto (1 + t/t_{\text{sc}})^{-4}$, and we write

$$E(x, t) = \mathcal{E}(x, t) E_0 \left[\frac{R_0}{R(t)} \right]^4 = E_0 \psi(x) \phi(t) \left[\frac{R_0}{R(t)} \right]^4, \quad (11)$$

where $\psi(x)$ describes the radial variation and $\phi(t)$, the temporal variation, and E_0 is the initial energy density.

The density can be written as

$$\rho(r, t) = \rho_0 \tilde{\rho}(x) \left[\frac{R_0}{R(t)} \right]^3, \quad (12)$$

where $\tilde{\rho}(x)$ is the radial profile of the density, normalized so that $\tilde{\rho}(0) = 1$.

The extinction coefficient χ is the mass-opacity coefficient κ times the density. We allow κ to have an intrinsic radial dependence, described by $\tilde{\kappa}(x)$, as well as a time dependence, $\zeta(t)$:

$$\chi(r, t) = \kappa_0 \tilde{\kappa}(x) \zeta(t) \rho_0 \tilde{\rho}(x) \left[\frac{R_0}{R(t)} \right]^3. \quad (13)$$

Separation of variables is possible only if the opacity does not depend upon the energy density (i.e., the temperature). Remarkably, conditions may actually conspire to produce an effective (flux mean) opacity that is roughly constant with both time and depth through the ejecta (Pinto & Eastman 2000a), though for now we will merely take this as an assumption in the derivation.

The volume energy deposition rate ϵ will scale as

$$\epsilon(r, t) = \frac{3M_{\text{Ni}} \epsilon_0}{4\pi R_0^3} \theta(t) \Lambda(x, t) \left[\frac{R_0}{R(t)} \right]^3, \quad (14)$$

where $\epsilon_0 = E_{\text{Ni}} + E_{\text{Co}} = 1.73 \text{ MeV} + 3.69 \text{ MeV} = 5.42 \text{ MeV}$ is the total energy available from decay, per atom of ^{56}Ni , and $\Lambda(x, t)$ is the dimensionless energy-deposition function that results from γ -ray transport and escape. The total production rate of decay energy as a function of t is described by $\theta(t)$, given as

$$\theta(t) = \epsilon_0^{-1} \times \left[E_{\text{Ni}} e^{-t/\tau_{\text{Ni}}} + \frac{E_{\text{Co}} \tau_{\text{Co}}}{\tau_{\text{Ni}} + \tau_{\text{Co}}} (e^{-t/\tau_{\text{Co}}} - e^{-t/\tau_{\text{Ni}}}) \right]. \quad (15)$$

It is convenient to define the total energy available from the $^{56}\text{Ni} \rightarrow ^{56}\text{Fe}$ decay chain (excluding neutrinos) in terms of the total kinetic energy of the gas,

$$\tilde{\epsilon} = \frac{3M_{\text{Ni}} \epsilon_0}{4\pi R_0^3 E_0}, \quad (16)$$

and the initial diffusion time from the center as

$$\tau_d = \frac{3\chi_0 R_0^2}{c}, \quad (17)$$

where $\chi_0 = \rho_0 \kappa_0$.

Substituting equations (11), (12), (13), (14), and (15) into equation (10) gives

$$\tau_d \zeta(t) \frac{R_0}{R(t)} \phi \psi - \phi \frac{1}{x^2} \frac{\partial}{\partial x} \left(\frac{x^2}{\tilde{\chi}} \frac{\partial \psi}{\partial x} \right) = \tau_d \tilde{\epsilon} \zeta(t) \theta(t) \Lambda(x, t), \quad (18)$$

where we have combined the spatial shape of the density and opacities into the function $\tilde{\chi}(x) = \tilde{\rho} \tilde{\kappa}$. Equation (18) is the principle equation that describes the evolution of the radiation-field energy density.

Next we must specify the boundary conditions. At the center there is a reflection boundary condition where the flux vanishes, or equivalently, $\psi'(0) = 0$. At the surface, we use a solution to the plane-parallel gray-atmosphere problem, assuming that the thickness of the surface layers is small compared with the radius. This can be expressed as

$$\psi(x) = \frac{3}{4} \psi_e \left(\tau + \frac{2}{3} \right); \quad (19)$$

the $\frac{2}{3}$ comes from the Eddington approximation. At the outer edge, $\tau = 0$, and we have

$$\psi(1) = \frac{1}{2} \psi_e \quad (20)$$

and thus

$$\psi(x) = \frac{3}{2} \psi(1) \left[\tau(x) + \frac{2}{3} \right]. \quad (21)$$

The boundary condition is then

$$\psi(1) = \frac{2}{3} \left. \frac{d\psi}{dx} \right|_{x=1} \left(\left. \frac{d\tau}{dx} \right|_{x=1} \right)^{-1}. \quad (22)$$

Since the optical depth to the surface from radius r is

$$\begin{aligned} \tau &= - \int_r^{R(t)} \rho \kappa dr \\ &= - \rho_0 \kappa_0 R(t) \int_x^1 \tilde{\rho}(x') \tilde{\kappa}(x') dx', \end{aligned} \quad (23)$$

we have

$$\left. \frac{d\tau}{dx} \right|_{x=1} = - \rho_0 \kappa_0 R(t) \tilde{\rho}(1) \tilde{\kappa}(1). \quad (24)$$

It is more convenient to require the solution to go to zero at some radius beyond $x = 1$ as a boundary condition. Extrapolating equation (24) linearly, we find that this is equivalent to requiring $\psi(x_0) = 0$ at

$$x_0 = 1 - \frac{2}{3} \left. \frac{dx}{d\tau} \right|_{x=1}. \quad (25)$$

The value of x_0 increases as density declines, and strictly speaking, this will introduce into the spatial solution a time dependence that violates the conditions making equation (18) separable. However, if we consider this to be a slow, quasi-static change, the solution obtained by separation of variables is not too inaccurate, and will be adequate for our needs. We will touch on this again below.

To solve equation (18), we follow the usual procedure for separation of variables and first find a solution to the homogenous equation, where energy deposition from decay is set to zero. In the absence of any sources, equation (18) can be written as

$$\frac{R_0}{R(t)} \tau_d \zeta(t) \frac{\phi}{\psi} = \frac{1}{x^2} \frac{\partial}{\partial x} \left(\frac{x^2}{\tilde{\chi}} \frac{\partial \psi}{\partial x} \right). \quad (26)$$

Since the terms on the left-hand side of this equation depend only on t , while those on the right-hand side depend only on x , each must be equal to a constant independent of either x or t . Let this constant be α . We can then write, for the spatial part,

$$\frac{1}{x^2 \psi(x)} \frac{\partial}{\partial x} \left(\frac{x^2}{\tilde{\chi}} \frac{\partial \psi}{\partial x} \right) = -\alpha. \quad (27)$$

For $\tilde{\chi} = 1$, the solution can be written

$$\psi(x) = \frac{\sin(\alpha^{1/2} x/x_0)}{\alpha^{1/2} x/x_0}, \quad (28)$$

where the eigenvalue α depends upon the total optical depth. For large opacity, $d\tau/dx$ is large, and the boundary condition equation (24) approaches the radiative-zero condition, $\psi(1) = 0$. For constant χ , the radiative-zero eigenvalues are $\alpha_n = n^2 \pi^2$, and the eigenfunctions are

$$\psi_n(x) = \sqrt{2} \frac{\sin(n\pi x)}{x}. \quad (29)$$

Given α_n , the temporal part of the solution, $\phi_n(t)$ is determined by the homogenous equation

$$\frac{R_0}{R(t)} \tau_d \zeta(t) \frac{\phi_n}{\phi_n} = -\alpha_n. \quad (30)$$

For $\zeta(t) = 1$ (opacity does not change with time), the solution can be written as

$$\phi_n(t) = \exp \left[- \frac{\alpha_n t}{\tau_d} \left(1 + \frac{t}{2t_{sc}} \right) \right]. \quad (31)$$

When $\tilde{\chi}$ is an arbitrary function, there are no analytic solutions to equation (27), and we must determine the eigenfunctions numerically. Eigenvalues are determined by a Rayleigh-Ritz procedure, and a discrete representation of their corresponding eigenfunctions is obtained by relaxation. The basin of convergence to a desired eigenfunction for this process is surprisingly small; for most interesting $\tilde{\rho}(x)$, eigenvalues must be determined to better than a percent for the resulting relaxation to converge to the desired solution. We prefer to normalize the solutions such that the functions ψ_n are orthonormal with respect to the inner product

$$\langle f | g \rangle \equiv \int_0^1 f(x) g(x) x^2 dx. \quad (32)$$

As the solution progresses in time, the spatial solution changes, because the value of x_0 increases with decreasing optical depth. To avoid the need of a new solution of equation (27) at each time, in much of the discussion that follows, we will take the radiative-zero solution. This allows a single set of eigenvalues to be used at all times. For more realistic calculations, we note that the change in eigenvalues due to changes in $\tilde{\chi}$ over time is slow and continuous. We may thus continuously re-solve the eigenvalue problem as we evolve the solution in time. As an example, Table 1 lists the first 25 eigenvalues for the radiative-zero solution with $\tilde{\chi} = e^{-kx}$, with $k = 0-4$. A selection of these functions is shown in Figure 1.

Turning now to our original, inhomogeneous transport equation, equation (18), the general solution for $E(x, t)$ is an

TABLE 1
EIGENVALUES FOR $\rho(x) = e^{-kx}$

Mode	$k = 0$	$k = 1/4$	$k = 1/2$	$k = 1$	$k = 2$	$k = 4$
1.....	9.8696 ₀	1.1878 ₁	1.4250 ₁	2.0298 ₁	3.9256 ₁	1.1637 ₂
2.....	3.9478 ₁	4.5567 ₁	5.2460 ₁	6.9007 ₁	1.1596 ₂	2.9175 ₂
3.....	8.8827 ₁	1.0152 ₂	1.1573 ₂	1.4922 ₂	2.4089 ₂	5.6453 ₂
4.....	1.5791 ₂	1.7978 ₂	2.0414 ₂	2.6115 ₂	4.1477 ₂	9.3937 ₂
5.....	2.4674 ₂	2.8037 ₂	3.1773 ₂	4.0488 ₂	6.3781 ₂	1.4181 ₃
6.....	3.5531 ₂	4.0328 ₂	4.5651 ₂	5.8043 ₂	9.1012 ₂	2.0015 ₃
7.....	4.8362 ₂	5.4852 ₂	6.2050 ₂	7.8782 ₂	1.2317 ₃	2.6900 ₃
8.....	6.3167 ₂	7.1610 ₂	8.0969 ₂	1.0271 ₃	1.6027 ₃	3.4837 ₃
9.....	7.9946 ₂	9.0602 ₂	1.0241 ₃	1.2982 ₃	2.0230 ₃	4.3828 ₃
10.....	9.8700 ₂	1.1183 ₃	1.2637 ₃	1.6011 ₃	2.4927 ₃	5.3874 ₃
11.....	1.1943 ₃	1.3529 ₃	1.5285 ₃	1.9360 ₃	3.0117 ₃	6.4974 ₃
12.....	1.4213 ₃	1.6098 ₃	1.8186 ₃	2.3027 ₃	3.5802 ₃	7.7130 ₃
13.....	1.6681 ₃	1.8891 ₃	2.1338 ₃	2.7013 ₃	4.1980 ₃	9.0342 ₃
14.....	1.9346 ₃	2.1907 ₃	2.4743 ₃	3.1317 ₃	4.8653 ₃	1.0461 ₄
15.....	2.2208 ₃	2.5147 ₃	2.8400 ₃	3.5941 ₃	5.5819 ₃	1.1993 ₄
16.....	2.5269 ₃	2.8610 ₃	3.2309 ₃	4.0883 ₃	6.3480 ₃	1.3632 ₄
17.....	2.8526 ₃	3.2297 ₃	3.6471 ₃	4.6144 ₃	7.1635 ₃	1.5375 ₄
18.....	3.1981 ₃	3.6207 ₃	4.0885 ₃	5.1724 ₃	8.0284 ₃	1.7225 ₄
19.....	3.5634 ₃	4.0341 ₃	4.5551 ₃	5.7624 ₃	8.9428 ₃	1.9180 ₄
20.....	3.9484 ₃	4.4699 ₃	5.0469 ₃	6.3842 ₃	9.9066 ₃	2.1241 ₄
21.....	4.3532 ₃	4.9279 ₃	5.5640 ₃	7.0379 ₃	1.0920 ₄	2.3408 ₄
22.....	4.7778 ₃	5.4084 ₃	6.1063 ₃	7.7235 ₃	1.1983 ₄	2.5680 ₄
23.....	5.2221 ₃	5.9112 ₃	6.6739 ₃	8.4410 ₃	1.3095 ₄	2.8059 ₄
24.....	5.6862 ₃	6.4364 ₃	7.2667 ₃	9.1905 ₃	1.4256 ₄	3.0543 ₄
25.....	6.1700 ₃	6.9840 ₃	7.8848 ₃	9.9719 ₃	1.5467 ₄	3.3133 ₄
Ratio.....	1.0	1.1322	1.2782	1.6163	2.5063	5.3643

NOTE.—The first 25 eigenvalues for the spatial equation (27) The final row is the ratio of subsequent eigenvalues to $n^2\pi^2$, the asymptotic limit.

expansion in terms of the eigenfunctions ψ_n :

$$E(x, t) = \sum_{m=1}^{\infty} E_m \psi_m(x) \phi_m(t). \quad (33)$$

If we substitute this expansion into the inhomogeneous equation (18), multiply by $x^2\psi_n(x)$, and integrate from $x = 0$ to 1, we get

$$\dot{\phi}_n + \frac{\alpha_n}{\tau_d} \left(1 + \frac{t}{t_{sc}}\right) \zeta(t)^{-1} \phi_n = \tilde{\epsilon}\theta(t) \left(1 + \frac{t}{t_{sc}}\right) \langle \Lambda | \psi_n \rangle, \quad (34)$$

where $\langle \Lambda | \psi_n \rangle$ is the overlap integral of $\Lambda(x, t)$ with eigenfunction $\psi_n(x)$ according to equation (32).

For simple forms of $\zeta(t)$ and $\langle \Lambda | \psi_n \rangle$, equation (34) can be integrated analytically. It is, however, a straightforward matter to integrate this equation numerically, and one need not be limited by the analytic integrability of these two functions.

We must now put back the dimensional constants in order to be able to calculate a light curve. Starting with the definition of the flux equation (eq. [9]), we have for the luminosity

$$L(t) = -\frac{4\pi c R_0 E_0}{3\chi_0} \frac{1}{\zeta(t)} \sum_{n=0}^{\infty} \phi_n(t) \left[\frac{x^2}{\tilde{\chi}(x)} \frac{d\psi}{dx} \right]_{x=1}. \quad (35)$$

Because the boundary conditions are $\psi(0) = 0$ and $\psi'(x_0) = 0$, there is no scale to the problem, and we are free to impose a third condition on the overall normalization of the solution. We can compare the luminosity with the energy deposited at late times by noting that when the time-scale over which the energy deposition $\theta(t)\Lambda(t, x)$ changes becomes long compared with the diffusion time, the ϕ_n go asymptotically to

$$\phi_n = \frac{\tau_d}{\alpha_n} \tilde{\epsilon}\theta(t)\zeta(t)\langle \Lambda | \psi_n \rangle. \quad (36)$$

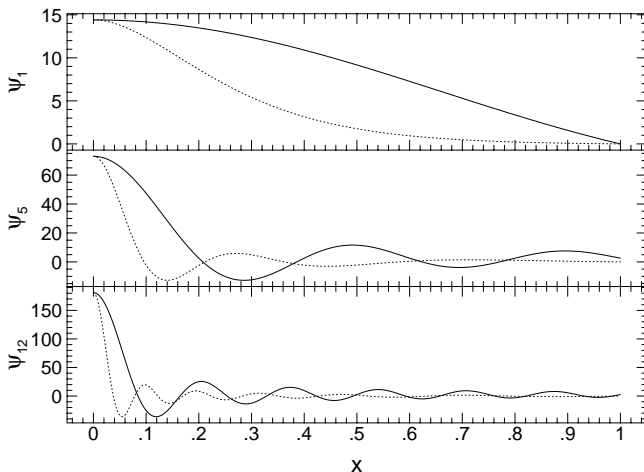


FIG. 1.—Eigenfunctions for mode numbers 1, 5, and 12 for exponential density laws with constant $k = 0$ and 4. The energy is more centrally condensed for the more centrally condensed structure (dotted lines).

If we integrate equation (27) over volume, we find that

$$\left[\frac{x^2}{\tilde{\chi}(x)} \frac{d\psi}{dx} \right]_{x=1} = -\alpha_n I_n(1), \quad (37)$$

where the total radiation energy interior to x is

$$I_n(x) = \int_0^x x^2 \psi_n dx. \quad (38)$$

Putting these two results into the expression for the luminosity and using the definitions of τ_d and $\tilde{\epsilon}$ gives

$$L(t) = 3M_{\text{Ni}} \epsilon_0 \theta(t) \sum_{n=0}^{\infty} \phi_n(t) \langle \Lambda | \psi_n \rangle I_n(1). \quad (39)$$

If $\Lambda(x, t)$ is constant in x , we can let $\Lambda(x, t) \sim \Lambda(t)$, and the sum becomes

$$\Lambda(t) \sum_{n=0}^{\infty} \left(\int_0^{x_s} x^2 \psi_n dx \right)^2. \quad (40)$$

Requiring that the solutions ψ_n be normalized such that this is $\Lambda(t)/3$ leads finally to

$$L(t) = M_{\text{Ni}} \epsilon_0 \theta(t) \Lambda(t), \quad (41)$$

the instantaneous energy deposition.

To examine the effect of including an increasing number of modes on the *shape* of the light curve, it is convenient to renormalize the energy deposition such that the correct total amount of energy is deposited per unit time into whatever modes are included in the calculation. We therefore divide the energy-deposition factor $\langle \Lambda | \psi_n \rangle$ by the quantity

$$f = \frac{\sum_n \langle \Lambda | \psi_n \rangle}{\int_0^1 x^2 \Lambda dx}. \quad (42)$$

This has the aliasing effect of overestimating the power in the included modes just enough to bring the deposited power to the correct value.

For the γ -ray deposition function, $\Lambda(x, t)$, we compute a numerical solution to the time-independent γ -ray line transport problem at each time t . It is not necessary to solve the fully time-dependent transport problem, because the flight time for γ -rays before absorption or escape is much smaller than any other timescale of interest. We have performed this calculation two ways: in one case, each of the most important lines in the ^{56}Ni and ^{56}Co decay spectra are separately transported, as described by Woosley et al. (1994). Alternatively, we perform the calculation for just two lines, one for ^{56}Ni at the emission-weighted mean energy of 479 keV, and the other for ^{56}Co , at the emission-weighted mean energy of 1.13 MeV. The two methods give results that agree with each other and with exact Monte Carlo results to better than a percent over the first 30–40 days of the light curve.

2.1. Comparison with a Multigroup Calculation

In order to assess the accuracy or realism of the analytic model, it is instructive to compare its predicted bolometric light curve with one produced by a more detailed (and expensive) calculation. We have therefore used the procedures outlined in the last section to compute the light curve of a model that approximates the main properties of the well-studied M_{ch} deflagration model W7 of Nomoto, Thielemann, & Yokoi (1984). For the analytic model, we take $M_{\text{tot}} = 1.39 M_{\odot}$, $M_{56} = 0.625 M_{\odot}$, $R_0 = 1.40 \times 10^8$ cm, and $v_{\text{max}} = 10^9$ cm s $^{-1}$. The peak light curve is insensitive to the choice of initial temperature, and the value 10^{10}

K was used. The density is constant with radius, and a radiative-zero boundary condition is assumed. The mean opacity was taken to be the constant value $\kappa_0 = 0.13$ cm 2 g $^{-1}$. The abundance of ^{56}Ni is unity out to a radius given by $r_{56} = (M_{56}/M_{\text{tot}})^{1/3}(R_0 + v_{\text{max}} t)$ and zero beyond that radius. The γ -ray deposition was computed as described above.

Figure 2 compares the analytic calculation with the bolometric light curve obtained by a multigroup (3000 frequency points) LTE transport calculation made with EDDINGTON (Eastman & Pinto 1993). The EDDINGTON calculation used the actual structure and composition of model W7 and predicted an average flux mean opacity equal to the value adopted for the gray calculation ($\kappa = 0.13$ cm 2 g $^{-1}$). For the first 30 days, the agreement between the two calculations is excellent. We note that the good agreement is somewhat deceptive, because the constancy of κ with time arises by assumption in the gray model, while no such assumption was made in the multigroup calculation (however, see Paper II—there is some reason to expect that the opacity will in fact be roughly constant with depth).

The “bump” in the light curve of the EDDINGTON calculation that appears between 30 and 44 days reproduces similar features seen in the observational data (Suntzeff 1995). It is caused by a decrease in the mean opacity, which allows stored energy to be released more quickly than in the constant-opacity models. The constant-opacity calculation lacks the second bump, and falls onto the radioactive tail more slowly as a result.

2.2. Thermal Conditions in a Maximum-Light SNe Ia and Parameter Sensitivity

One application of the analytic model is to estimate temperatures in SNe Ia. Figure 3 shows central temperature versus time for the analytic model previously shown in Figure 2. At times $t < 20$ days, the central temperature is $T(x = 0) > 13,000$ K, which puts the peak of the blackbody

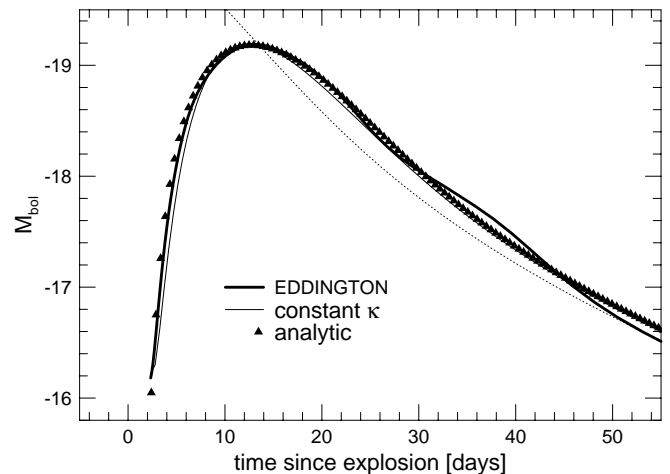


FIG. 2.—Comparison of the bolometric light curve (*solid line*) of model W7 of Nomoto et al. (1984) as determined by a multigroup radiation transport calculation performed with EDDINGTON, a numerical solution of the gray transport equation for the same model employing a constant opacity, and the analytic solution described in the text for a constant-density explosion of the same total mass, ^{56}Ni mass, kinetic energy, and opacity. The constant-opacity calculations agree well with the multigroup calculation with the exception of the secondary “bump” that is produced by a decrease in the mean opacity, thus allowing the release of stored energy on a shorter timescale than in the constant-opacity cases.

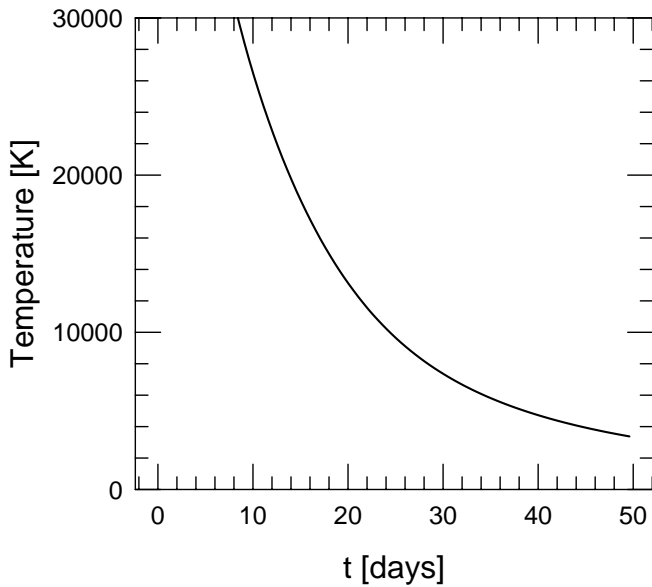


FIG. 3.—Analytic model temperature solution at $x = 0$ for a constant-density model having the same mass, kinetic energy, and ^{56}Ni mass as model W7.

spectrum at $\lambda_{\text{wein}} \lesssim 2200 \text{ \AA}$, a wavelength at which the optical depth due to lines is very large.

Figure 4 demonstrates the dependence of the analytic model's light-curve solution upon changes in opacity, the distribution of ^{56}Ni , the mass of ^{56}Ni , and the explosion energy, all for Chandrasekhar-mass explosions. In all these

calculations the fiducial model is the same—the “W7-like” model discussed in the previous section.

In the first panel of Figure 4, the opacity is varied by a factor of 2 above and below our fiducial model. The effect is just what one would expect. A lower opacity decreases the diffusion time, allowing radiation to escape earlier. Spending less time in the expanding, optically thick enclosure, the radiation suffers a smaller loss to expansion. The light curve thus peaks earlier, at a higher luminosity. The ejecta become optically thin sooner, making the transition to the asymptotic solution of balanced deposition and radiative loss at an earlier time, and the peak becomes narrower than the fiducial model. The higher-opacity model likewise peaks later, is fainter, and is considerably broader. Note that this behavior is the opposite of the LWR relation; at least for an opacity that is constant with time, we must look elsewhere for a fundamental parameter to explain observations. Note also that a factor of 4 change in opacity leads to only half a magnitude of difference in the peak magnitude.

Next we show the effect of varying the extent of the energy deposition, but without varying the mass of ^{56}Ni , the velocity, or the total mass of the explosion. Such a variation might be the result of hydrodynamically induced mixing, or it may be simply that little extra energy is liberated by burning beyond the Si group to ^{56}Ni . Models with more centrally condensed deposition peak later, but with only very slightly lower peak magnitude. The width of the peak is somewhat broader with a broader distribution of deposition, as there is a larger range in diffusion times for the deposited energy to make it to the surface.

We next vary the kinetic energy of the explosions, which is to say the scale velocity, by a factor of 2 above and below

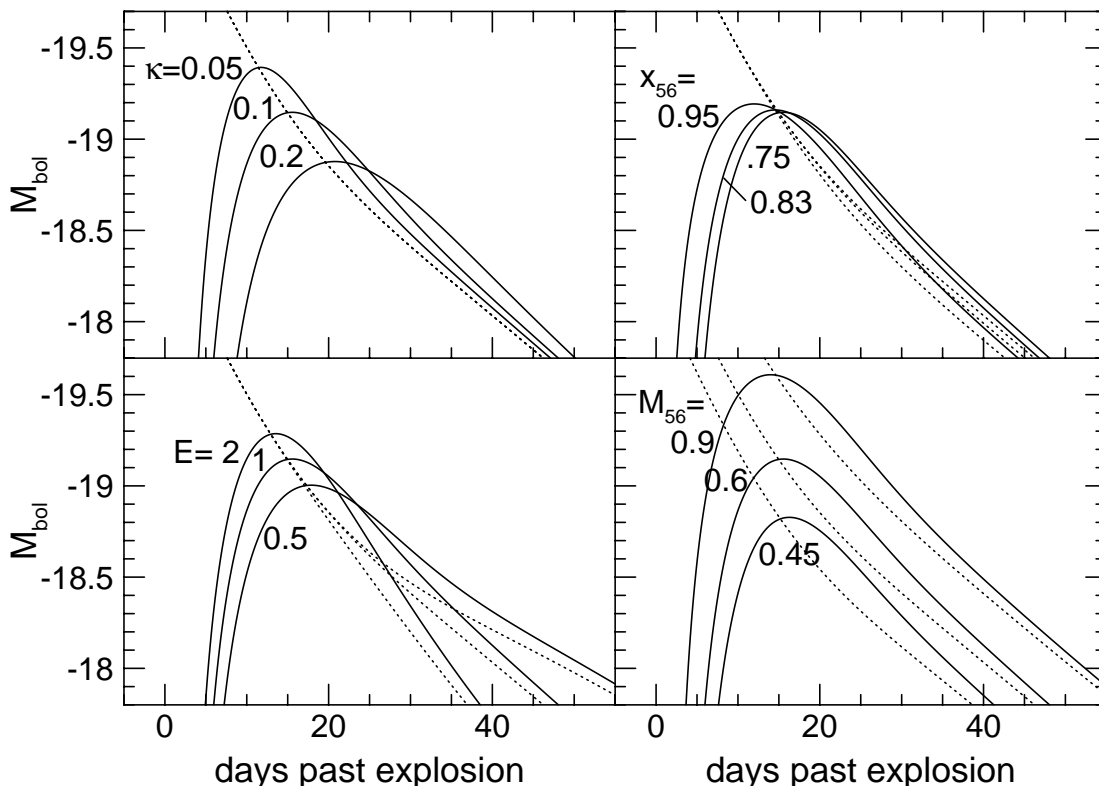


FIG. 4.—Effect of varying the opacity, extent of deposition, explosion energy, and ^{56}Ni mass on the standard explosion (center line in each plot). The instantaneous energy deposition rate is shown as a dotted line.

the fiducial model. Because a greater expansion velocity leads to a more rapid decline in column depth, more energetic explosions peak earlier, at higher luminosities, and decline more rapidly. Thus, an increase in explosion energy has much the same effect as a decrease in opacity. Indeed, the opacity and the density occur in the thermalized radiation equations only as the product $\rho\kappa$. The change in the slope of the energy deposition following peak is a consequence of the change in column depth to the γ -rays.

In the last panel of Figure 4, the ^{56}Ni mass is varied. The peak luminosity is seen to follow the ^{56}Ni mass, with a slight change in shape arising from the varying fraction of the supernova filled with radioactive material as in the second panel.

Arnett's (1982, 1996) analytic SNe Ia light-curve model predicts that the luminosity at bolometric maximum would precisely equal the instantaneous rate of deposition from ^{56}Ni and ^{56}Co decay. This has provided some interesting constraints, both on the mass of ^{56}Ni produced and on the luminosity at maximum. "Arnett's rule," as it has come to be known, is only approximate, however, and is related to the assumptions that a single eigenmode describes the shape of the energy density and that the energy deposition has this same shape.

Figure 5 illustrates the result of including a varying number of eigenmodes in the solution. Arnett's (1982) result is reproduced by taking only the first mode. The effect of including higher modes is primarily to steepen the rise to

peak and to broaden the width of the peak. From equation (34), we see that the e -folding time for the power in mode n to decay is proportional to the eigenvalue, which varies roughly as the square of the mode number. This is easy to understand physically. The higher order modes describe variations of the energy density on smaller and smaller spatial scales. The energy variations at these scales do not have far to go to diffuse out to a smoother distribution, so the power in these modes declines rapidly. In the lower panel of the figure, we have used the same model as in Figure 2, while in the upper panel we have made the energy deposition uniform over the entire star. In both cases, the effect of adding more modes is to steepen the rise to peak. In the case with the ^{56}Ni "buried" well within the ejecta, the energy from the decay takes more time to diffuse to the surface, and by the time it does, the fundamental mode has most of the power. Thus, the time of peak and the peak magnitude are but little affected by the number of modes. For the uniform-deposition case in the upper panel, however, there is deposition near the surface, which can be represented adequately only by the inclusion of higher eigenmodes. The energy deposited near the surface spends less time diffusing and suffers less from adiabatic decompression. Thus, the inclusion of the higher modes shortens the rise time. The light curve peaks earlier and at a higher luminosity. Because of this effect, all subsequent light curves in this work are calculated with a sufficient number of eigenmodes to approach the exact solution. On the other hand, the figure shows that for models in which the ^{56}Ni does not extend beyond, say, 85% of the radius, the distribution of radioactivity has little effect on the light curve. By the time energy has diffused out to the surface, information about this distribution has been lost.

The tendency toward the fundamental mode near maximum provides a clue to the expected shape of the peak. For a constant opacity and times that are long compared with the scale time, we see from equation (31) that the peak of the light curve will be a Gaussian,

$$\phi(t) = \exp\left(-\frac{\alpha_1 t^2}{2t_{sc} \tau_d}\right). \quad (43)$$

This provides a theoretical justification for the use of a Gaussian as a fitting function by Vacca & Leibundgut (1996) to determine the rise time and width of observed light curves. For explosions with significant amounts of ^{56}Ni near the surface, this approximation will of course be less accurate. In such cases, a larger number of eigenmodes are necessary to describe the wider variation of diffusion times from the sites of deposition to the surface.

The previous figures also show that, except for models with significant deposition near the surface, the luminosity at peak is nearly identical to the instantaneous deposition rate (under the assumption of an opacity that is constant with time, $d\zeta/dt = 0$), as first noted by Arnett (1982). It is important to remember that this does *not* imply a short diffusion time at peak. Rather, it results from the fact that peak light is the watershed that separates times at which the energy deposition rate is greater than the luminosity from those at which it is less, as noted in the introduction to this section.

In Figure 6 we show the effect of altering the density structure of the supernova. The density of most SN Ia models is represented fairly well by an exponential in veloc-

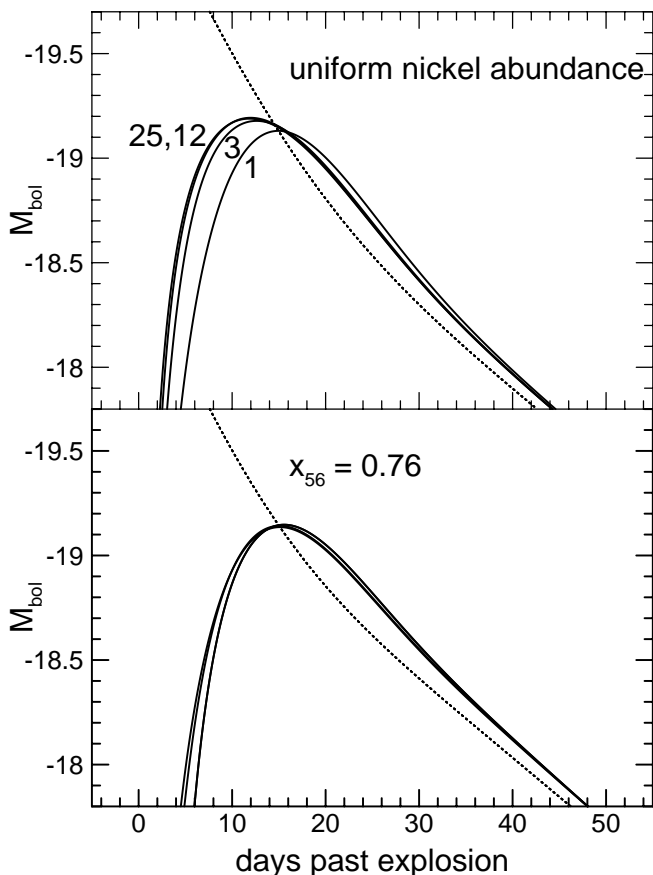


FIG. 5.—Effect of the number of eigenmodes on the calculated light curve. In the upper panel, energy deposition is taken to be uniform with radius. In the lower, the deposition extends out to the radius used in the standard model, $x = 0.76$.

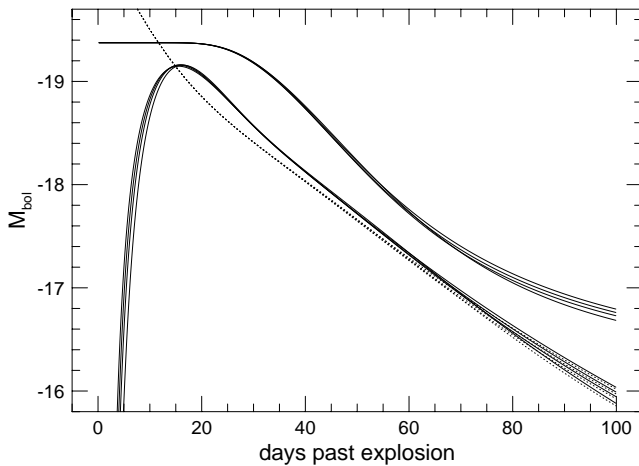


FIG. 6.—Light curve from a model with density structure $\tilde{\rho}(x) = \exp(-kx)$ plotted along with that of the constant-density fiducial model. The upper set of curves shows the time dependence of the energy-deposition fraction; for all density laws, the deposition is nearly complete until 10 days or so after peak.

ity, $\tilde{\rho}(x) = \exp(-kx)$ with $k \sim 4$, which departs fairly strongly from the constant-density profile we have employed thus far. One can see from the figure that in spite of the crudeness of the model, a constant-density model light curve is nearly identical to one that possesses a more realistic density profile. The light curve is insensitive to the density structure for the same reasons that it is insensitive to the number of included modes.

None of the parameters we have examined thus far can account for the luminosity-width relation; varying the explosion energy and opacity leads to a correlation *opposite* in sense to the “brighter implies broader” behavior observed, and the other parameters lead to little variation in light-curve shape. One way to obtain the LWR suggests itself immediately: if the mass of ^{56}Ni is decreased while the kinetic energy is increased, then a sufficient decrease in ^{56}Ni mass can offset the increased luminosity of the narrower peak. The problem with this proposition is that in a M_{ch} explosion, most of the star must be burned at least to the silicon/calcium group to obtain the observed velocities. We can lower the ^{56}Ni mass only by increasing the fraction of the star burned to Si/Ca. Even though approximately 75% as much energy is liberated in burning only to Si/Ca as in burning all the way to ^{56}Ni , it is hard to see how a decrease in ^{56}Ni fraction sufficient to achieve the desired effect on the light curve can accompany a sufficient increase in kinetic energy.

Another way to obtain the LWR in an M_{ch} explosion is to vary the opacity in such a way that an increased ^{56}Ni mass is accompanied by an increase in opacity enough to offset the increase in kinetic energy, as must be required from the results of Höflich & Khokhlov (1996). An increase in ^{56}Ni will in general result from a more energetic explosion and hence a narrower peak. If the opacity is increased sufficiently, however, the peak will be, nonetheless, broader. An increased opacity accompanying a higher ^{56}Ni mass might result from a combination of higher temperatures due to increased deposition and a higher opacity in iron group elements than in Si/Ca.

One can estimate crudely how much of an opacity increase is needed in order to reproduce the LWR relation,

using the fact that the rate of decline from maximum is a measure of the diffusion time,

$$t_{\text{diff}} \approx R^2 \rho \kappa \propto \frac{M \kappa}{v t} \propto \frac{M^{3/2} \kappa}{E^{1/2} t}, \quad (44)$$

where we have assumed the velocity $v \propto (E/M)^{1/2}$. Hamuy et al. (1995) give $\Delta M_{15} = 0.82$ and 1.72 (B magnitudes) for SN 1992bc and SN 1992bo, respectively, which correspond to diffusion times of 19.6 and 9.5 days, which, if we take that to be the ratio of their explosion energies, corresponds to an opacity ratio of 3.1.

The final parameter in the solution is the total mass of the explosion. For a constant velocity (specific kinetic energy), changing the total mass will result in a change in the density and will have a similar effect to changing the opacity as in Figure 4, leading to a brighter and narrower peak for lower masses. Lower mass explosions, however, will naturally produce less ^{56}Ni , as the densities attained in lower mass white dwarfs are smaller. Changing the density will also affect the γ -ray deposition. A decrease in mass will allow energy to escape more easily in the form of γ -rays. More importantly, it will allow the *rate* at which the escape increases to be greater, and this more rapid falloff in the deposition will also act to oppose the tendency toward increased luminosity in models with lower column depth.

In Figure 7, the total mass of the ejecta is varied. Simply as an illustration of the effects, in both panels the ^{56}Ni mass fraction is kept constant, but in the upper panel the energy of the explosion is kept constant while in the lower panel the ratio of explosion energy to total mass, the specific energy, and thus the velocity, are preserved. Constant-energy series of explosions might arise, for example, from the fact that lower mass white dwarfs have lower densities, leading to an increasing fraction of the energy arising from incomplete burning to lighter nuclei. Explosions with constant specific energies would arise when different mass progenitors nonetheless give similar nucleosynthetic yields. In both cases, the higher column depth of larger mass models leads to later, broader peaks, but the larger adiabatic losses are more than compensated by the increased mass of ^{56}Ni . In both cases, larger masses lead to brighter and broader peaks, as observed.

While such an explanation for the LWR is attractively simple, it is not clear how progenitors of varying mass might lead to SNe Ia explosions. Two possibilities have been suggested. The first are low-mass ($0.6\text{--}1.0 M_{\odot}$) C/O cores that have accreted helium on their surfaces to the point where the helium detonates (Woosley & Weaver 1994; Livne & Arnett 1995). This helium detonation will likely lead, in many circumstances, to a detonation of the C/O core as well, resulting in a supernova with a total mass less than M_{ch} . Such models as have been computed to date for such a scenario do not show encouraging agreement with spectral observations, but the model has not been exhaustively explored. The second possibility is that SNe Ia are the result of mergers between lower mass C/O cores. This would also lead to a variety of explosion masses. Because of the computational difficulty involved in a simulation of this inherently multidimensional process, there have been no models to date that have been carried to a point from which a spectrum or light curve might be computed.

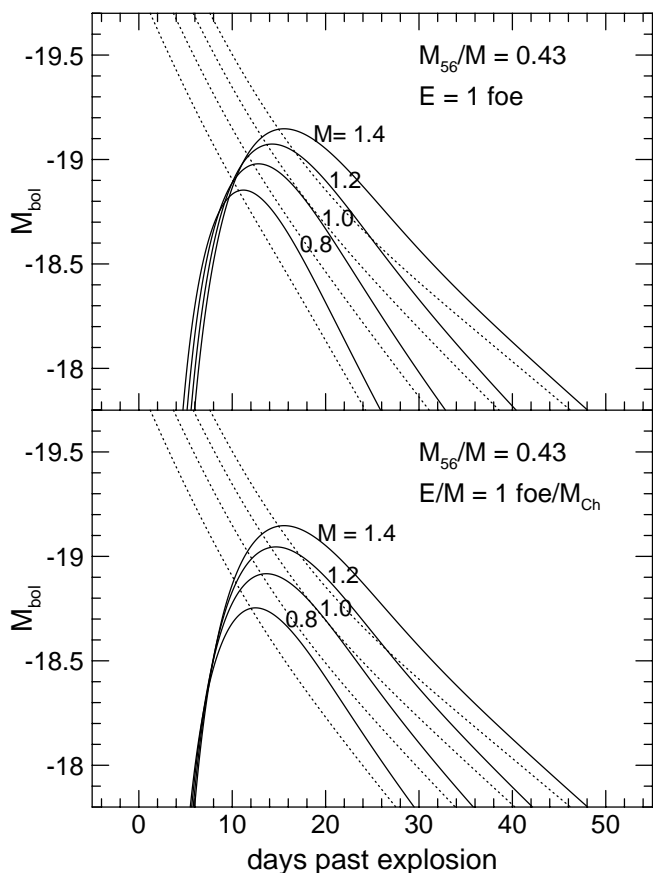


FIG. 7.—Two ways of varying the total mass of the explosion: in the top panel the explosion energy is constant at 1 foe (10^{51} ergs), and the ^{56}Ni yield is fixed as a constant fraction of the total mass, for $M = 0.8, 1.0, 1.2,$ and $1.4 M_{\odot}$. In the lower panel E/M is held constant at 3.6×10^{17} ergs g^{-1} .

In the absence of detailed models, then, we can note only that explosions of differing masses would appear to provide a simple and natural explanation for the physics underlying the LWR, with the total mass of the explosion as a fundamental underlying parameter. At present, a variation in opacity accompanying variations in ^{56}Ni mass seems more likely.

3. TIME DEPENDENCE

As a final, more technical issue, we can use the analytic solution we have developed to examine the validity of various approximations to the solution of the radiative transfer problem in supernovae. While it may seem obvious that SNe Ia are not steady state phenomena, several papers have appeared in the literature in which the absolute luminosity of some SNe Ia has been estimated ignoring the basic time dependence of the transport physics. This is a natural and indeed necessary assumption for the calculation of NLTE (non-LTE) maximum-light spectra, as general, time-dependent, NLTE calculations are beyond current computational capabilities. It is, however, important to understand the magnitude of the errors that may be incurred by such approximations.

Among the most important and commonly used approximations is that of *steady state*—that one or more of the time-dependent terms in equations (1) and (2) can be ignored. These are enormously attractive approximations,

as they greatly reduce the computational complexity. A time-independent problem is much easier to solve than a time-dependent one!

Steady state amounts to the assertion that heating by energy deposition and cooling by radiative processes (and perhaps by expansion as well) are balanced *at all times*. There are two versions of this approximation. The first asserts that the Lagrangian derivative (the first term in eq. [1]) is small compared with the flux divergence. In this approximation, the supernova is no different than a static stellar atmosphere. The second (employed, for example, by Nugent et al. 1995 and references therein), takes into account energy loss from PdV work but asserts that the Eulerian derivative $\partial E/\partial t$ is negligible.

In Figure 8 we present ratios of various terms in the transfer equations as functions of time for our fully time-dependent solution. For clarity, only the fundamental mode is considered; the inclusion of higher modes will make the time dependence different at different depths in the ejecta but does not alter the character of the solution or the order of magnitude of the terms.

The ratio of the Lagrangian derivative to the flux divergence in equation (1) is

$$\frac{DE}{Dt} \left[-\frac{1}{r^2} \frac{\partial}{\partial r} (r^2 F) \right]^{-1} = \psi \left[-1 + \frac{\tau_d}{\alpha} \frac{\tilde{\epsilon} \theta \Lambda}{\phi} - \frac{4\tau_d}{t_{sc} \alpha} \left(1 + \frac{t}{t_{sc}} \right)^{-2} \right]. \quad (45)$$

Using the asymptotic value equation (36), equation (45) becomes the ratio of the diffusion (current) time to the expansion (elapsed) time and thus goes to zero in the limit of large t . At late times, energy is deposited in the ejecta and is immediately radiated away; thus, the flux divergence must equal the deposition, and it is appropriate to use a “steady state” solution, which balances instantaneous luminosity against the time-varying deposition rate, $\theta(t)\Lambda(t)$.

At peak light, $\dot{\phi} = 0$ in equation (34) and in equation (36) as well, so equation (45) becomes the ratio of the present diffusion time to the elapsed time. Since peak occurs when the diffusion time approximately equals the elapsed time,

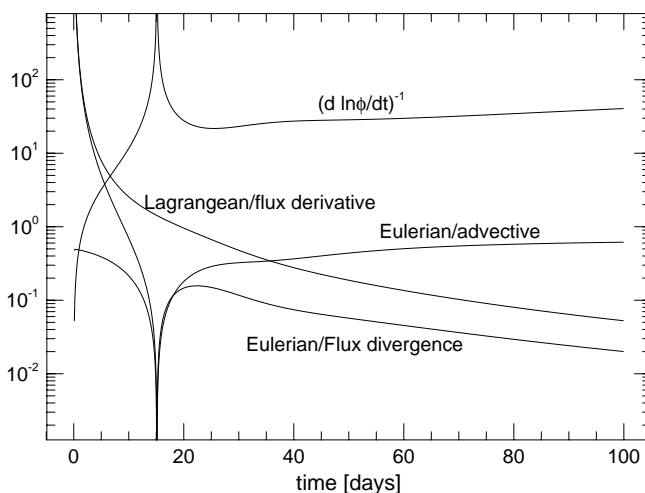


FIG. 8.—Ratios of various terms in the transfer equation as functions of time. Because a logarithmic scale is used, the absolute value of each curve is plotted. Thus, at maximum (near 15 days), the Eulerian derivative changes sign from positive to negative.

the ratio in equation (45) is ~ 1 , implying that the time-dependent terms cannot be ignored. Thus, while steady state is a fine approximation at late times, it is quite a poor approximation at earlier phases of the light curve. Indeed, for the “standard model” above, it is only after 246 days that the ratio in equation (45) falls below 1%.

In the second approximation, which one might call “quasi-steady state,” only the Eulerian derivative is neglected. We can formulate the ratio of the Eulerian to the advective derivative as

$$\frac{\partial E/\partial t}{(v \cdot \nabla)E} = \frac{t_{sc}}{4} \left[\frac{\tilde{\epsilon}\theta\Lambda}{\phi} - \frac{\alpha}{\zeta(t)/t_d} \right] \left(1 + \frac{t}{t_{sc}} \right)^2. \quad (46)$$

Once again, this ratio goes to zero in the limit of large time, but it also goes to zero at peak, when $\dot{\phi} = 0$. That this must be so is obvious from examination of the light curves of the previous sections. Before peak, the luminosity of the supernova is less than the rate at which energy is being deposited in the ejecta, even accounting for losses due to expansion. Shortly after peak, the luminosity is greater than the deposition rate. This means that before peak, a store of energy is being built up in the supernova and therefore that $\partial E/\partial t > 0$. After peak, this “excess” energy is radiated away, and the energy loss is greater than the loss due to expansion alone, so $\partial E/\partial t < 0$. Since the sign of the Eulerian derivative changes when the supernova traverses peak light, there must be a time near peak at which it is zero. This does not mean that the term can be ignored, however. When the effects of all modes are included, the time at which $\partial E/\partial t = 0$ is different for each radius. As well, the derivative’s value is changing rapidly; one can see from the figure that only a few days before and after maximum it is 30% as great in magnitude as the advection term.

We wish particularly to draw attention to the erroneous conclusions drawn in this regard by Baron, Hauschildt, & Mezzacappa (1996). In that work, its authors express $\partial E/\partial t$ as a finite difference over a time interval δt . They then go on to show that inclusion of this term has the effect of an additional source or sink of radiation. While this is correct, when comparing the magnitude of various terms, they let δt —which would be the “time step” in a finite-difference treatment of the time-dependent problem—be the *elapsed* time. They then conclude that the term is small and can be ignored. This is wrong. While it is obvious that in an implicit-difference scheme one approaches some sort of steady state if a sufficiently long time step is employed, it is equally obvious that such a state need have little semblance to a correct solution of the time-dependent equations. This is especially so in that the solution at peak is not an asymptotic limit. If they had chosen a time step small enough to preserve accuracy in the finite difference, δt would have been almost 2 orders of magnitude smaller and their estimate of the relative size of the Eulerian derivative would have been much the same as that determined here.

To see the error in the quasi-steady state approximation another way, consider the limiting case of infinite opacity, radiative equilibrium, and homologous expansion. Equations (1) and (2) then become

$$\frac{DE}{Dt} = -\frac{4\dot{R}}{R} E. \quad (47)$$

If we solve this equation directly, we find the expected result that $E \propto t^{-4}$. This clearly contradicts the notion that the

intrinsic time derivative of E is zero! In yet another demonstration, if we consider the case in which we set $\dot{\phi} = 0$, the light curve must decline monotonically, following the energy deposition. Thus, the mere fact that the light curve is observed to peak is testament to the error of the quasi-steady state.

Perhaps the simplest way to gauge the effects of time dependence upon the light curve is to examine when the luminosity emitted at a given time was deposited in the ejecta. Figure 9 shows the cumulative fraction of luminosity at maximum light as a function of deposition time for a typical supernova model. It is clear that the “residence time” of the energy that emerges from a supernova near maximum light is significant. From the figure, for example, 50% of the luminosity is energy deposited at times earlier than 75% the age of the supernova.

Energy is stored predominantly in the form of photons diffusing out through the ejecta. Even the tactic of taking the thermal structure of the matter from a light-curve calculation, placing it in an atmosphere code, and calculating the resulting spectrum does not do justice to the presence of these “old photons.” There is no reason to suspect that the radiation temperature is the same as the matter temperature, and thus, without taking some measure of the radiation-field energy density from the light-curve calculation, there is no way to characterize the spectrum or intensity of these photons in the spectrum calculation. The only way to avoid a serious omission in the physics of spectrum formation is to provide some measure of the spectral shape and intensity of the “old photons” to the atmosphere code. In practice, this means that the spectrum formation problem *is* the light-curve problem; one cannot avoid the inherent time dependence in calculating either light curves or spectra. Especially when attempting to calibrate SNe Ia as cosmological distance indicators, it is necessary to include all of these important physical effects.

It is true, however, that $\partial E/\partial t$ becomes small near maximum light, and it may be true, despite the presence of “old photons,” that a “quasi-steady state” treatment may not be too much in error at this epoch. Without a benchmark time-dependent NLTE calculation with which to compare, however, it is difficult to assess the magnitude of any error in the resulting luminosity. Since the spectrum-

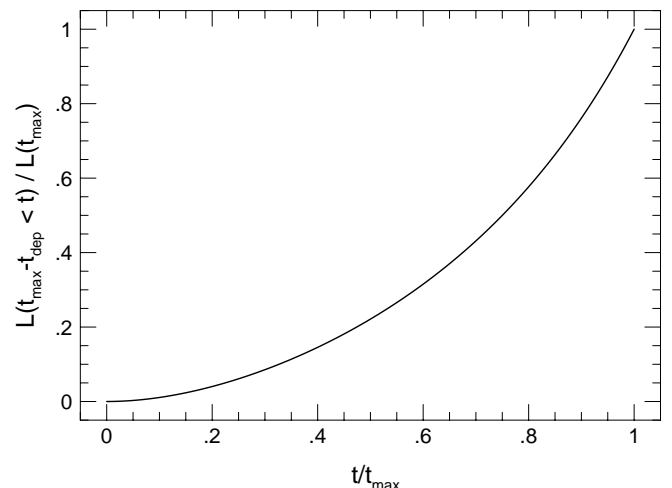


FIG. 9.—Fraction of maximum-light luminosity arising from energy deposited before the time indicated on the abscissa.

forming layers of the outer atmosphere are primarily scattering, and since the shape of the pseudocontinuum may have little to do with the gas temperature or the luminosity as demonstrated above, a good agreement with the observed spectrum *shape* may not in fact imply a reliable estimate of the luminosity.

4. CONCLUSIONS

We have derived an analytic solution of the comoving frame transport equations that closely reproduces the results of more complex numerical solutions. This allows one to examine a number of key features of the light-curve physics itself and of the observed systematics in SNe Ia data. One result is the demonstration that the light-curve and spectrum problem is inherently time dependent and cannot be approximated by time-independent calculations before at least 70 days past explosion.

Using the analytic model, we have explored the effect of changes in a variety of parameters on the resulting light curve. These include the opacity, explosion energy, ^{56}Ni mass and distribution, and total mass. Of these, there is only one parameter that by itself can explain the observed correlation of peak width and luminosity: the total mass. All others, when varied individually, lead to *anticorrelations*. This does not necessarily imply that the mass of the explo-

sion is *the* controlling parameter; there may be various combinations of parameters that, when altered in concert, lead to the same behavior. For example, if the opacity can be shown to be a strong function of the ^{56}Ni mass, then the behavior of models at a single mass may be able to reproduce the LWR. The fact that variations in so fundamental a property of the explosion as the total mass *can* explain the observed behavior is suggestive.

This work was supported (P. A. P.) by the National Science Foundation (CAREER grant AST9501634), by the National Aeronautics and Space Administration (grant NAG 5-2798), and by the U.S. Department of Energy (W-7405-ENG-48). Philip Pinto gratefully acknowledges support from the Research Corporation through a Cottrell Scholarship and from the General Studies Group at Lawrence Livermore National Laboratory. This work was begun at the European Southern Observatory, Garching bei München, where both P. A. P. and R. G. E. gratefully acknowledge support from the visitors program. Finally, we wish to thank W. D. Arnett, E. Baron, W. Benz, A. Burrows, P. Höflich, R. P. Kirshner, B. Leibundgut, M. Mamuy, D. McCray, J. Spyromilio, T. A. Weaver, J. C. Wheeler, and S. E. Woosley for many helpful discussions and comments throughout the development of this work.

REFERENCES

- Arnett, W. D. 1980, *ApJ*, 237, 541
 ———. 1982, *ApJ*, 253, 785
 ———. 1996, *Supernovae and Nucleosynthesis* (Cambridge: Cambridge Univ. Press)
 Barbon, R., Benetti, S., Cappellaro, E., Patat, F., & Turatto, M. 1993, *Mem. Soc. Astron. Italiana*, 64, 1083
 Baron, E., Hauschildt, P. H., & Mezzacappa, A. 1996, *MNRAS*, 278, 763
 Eastman, R. G., & Pinto, P. A. 1993, *ApJ*, 412, 731
 Evans, R., van den Bergh, S., & McClure, R. D. 1989, *ApJ*, 345, 752
 Hamuy, M., et al. 1993, *AJ*, 106, 2392
 Hamuy, M., Phillips, M. M., Maza, J., Suntzeff, N. B., Schommer, R. A., & Avilés, R. 1995, *AJ*, 109, 2438
 Harkness, R. P. 1991, in *SN 1987A and Other Supernovae*, ed. J. Danziger & K. Kjær (Garching: ESO), 447
 Höflich, P., & Khokhlov, A. M. 1996, *ApJ*, 457, 500
 Höflich, P., Khokhlov, A. M., & Wheeler, J. C. 1995, *ApJ*, 444, 831
 Livne, E., & Arnett, D. 1995, *ApJ*, 452, 62
 Mihalas, D. 1978, *Stellar Atmospheres* (San Francisco: Freeman)
 Mihalas, D., & Mihalas, B. W. 1984, *Radiation Hydrodynamics* (Oxford: Oxford Univ. Press)
 Nomoto, K., Thielemann, F. K., & Yokoi, K. 1984, *ApJ*, 286, 644
 Nugent, P., Baron, E., Hauschildt, P. H., & Branch, D. 1995, *ApJ*, 441, L33
 Phillips, M. M. 1993, *BAAS*, 182, 2907
 Pinto, P., & Eastman, R. 2000a, *ApJ*, 530, 757 (Paper II)
 Pollas, C. 1994, in *Les Houches, Session MCMXC, Supernovae*, ed. R. M. S. Bludman & J. Zinn-Justin (Amsterdam: North-Holland), 769
 Suntzeff, N. B. 1995, in *IAU Colloq. 145, Supernovae and Supernova Remnants*, ed. R. McCray (Cambridge: Cambridge Univ. Press), 41
 Vacca, W., & Leibundgut, B. 1996, in *Thermonuclear Supernovae*, ed. R. Canal & P. Ruiz-Lapuente (Dordrecht: Elsevier), 65
 Weaver, T. A., Axelrod, T. S., & Woosley, S. E. 1980, in *Type Ia Supernovae*, ed. J. C. Wheeler (Austin: McDonald Observatory), 113
 Woosley, S. E., Eastman, R. G., Weaver, T. A., & Pinto, P. A. 1994, *ApJ*, 429, 300
 Woosley, S. E., & Weaver, T. A. 1986, *ARA&A*, 24, 205
 ———. 1994, *ApJ*, 423, 371